

*Full Paper*

## **Aerodynamic investigation and redesign of ceiling fan blades for enhanced energy efficiency**

**Muhammad Aaqib Afaq<sup>1</sup>, Adnan Maqsood<sup>1,\*</sup>, Shahid Ikramullah Butt<sup>2</sup>, Tauseef Tauqeer<sup>3</sup> and Ammar Hasan<sup>3</sup>**

<sup>1</sup> Research Centre for Modeling and Simulation, National University of Sciences and Technology, Islamabad, Pakistan 44000

<sup>2</sup> School of Mechanical and Manufacturing Engineering, National University of Sciences and Technology, Islamabad, Pakistan 44000

<sup>3</sup> School of Electrical Engineering and Computer Science, National University of Sciences and Technology, Islamabad, Pakistan 44000

\*Corresponding author, e-mail: [adnan@rcms.nust.edu.pk](mailto:adnan@rcms.nust.edu.pk)

*Received: 17 July 2015 / Accepted: 24 May 2017 / Published: 9 June 2017*

---

**Abstract:** Ceiling fans play a pivotal role in indoor cooling and thermal comfort. In this paper a computational framework, validated by experimental data, is presented for the design enhancement of ceiling fan blades with the objective of enhancing energy efficiency. A parametric study is performed by steady-state numerical simulation of three-dimensional airflow. Specifically, the parameters considered in the study are rake angle, bend angle and bend position. Rated air delivery, power consumption and service value at different rotational speeds are set as performance measure. The recommended geometry from the parametric study is tested and compared with the original geometry. The results indicate that airflow and service value increase by 21% and 54% respectively at 300 revolutions per minute and power consumption is reduced by 22%.

**Keywords:** ceiling fan, energy efficiency, computational fluid dynamics, blade optimisation

---

### **INTRODUCTION**

Ceiling fan is the most widely used electric appliance for providing indoor comfort in the tropical regions of the world. Several technology protagonists have launched investigations in the design improvement of ceiling fans to reduce energy consumption through experimental, empirical and computational approaches. Jain et al. [1] studied the flow field of a ceiling fan inside an empty room through a series of experiments. Different flow regions were identified in the room through

smoke visualisation. A comparative study was conducted for the fan blades with and without winglets to improve the air circulation inside the room. The idea was to reduce any induced flow generated at the tips of the fan blades by suppressing the blade tip vortices. Due to spikes and winglets, the downward air velocity was increased by 13% with the same power consumption.

Schmidt and Patterson [2] experimentally compared the performance of fan blade designs. A prototype of fan with four blades was developed with a high angle of attack that achieved the rated airflow at 140 revolutions per minute (rpm) as compared to the conventional ceiling fan that delivers the same airflow at 270 rpm. An aerodynamically efficient fan blade was developed by incorporating various design features such as blade profile, geometric twist and taper ratio. The study concludes that the new ceiling fan design can decrease the power consumption by a factor of up to three as compared to the conventional ceiling fans.

Ramadan and Nader [3] investigated flow features of air in a room. The focus of the study was on numerical simulations of fluid flow. A finite-element-based commercial code was used to simulate the flow. Results showed that the flow pattern has a different feature as airflow crosses the fan disk and moves towards the floor. The considered configuration consisted of a simple ducted fan inside a room. The air flow variation and swirl behaviour were also investigated. It had a divergence angle of almost  $150^{\circ}$ . The computational data were compared with the experimental work of Jain et al. [1]. The authors reported a loss of flow momentum as air moved outside the fan diameter.

Momoi et al. [4] experimentally and computationally measured the air velocity around a ceiling fan in a large room. The fan speed was fixed at 160 rpm. The study suggested that the distance between ceiling fan and floor has a significant effect on the air flow inside the room. Parker et al. [5] proposed a fan blade design with a positive twist at the blade root and rounded tip. This new design doubled the airflow and gave less vibration, less noise and high energy efficiency at low speed ranges.

Lee et al. [6] numerically optimised the low-speed axial fan through response surface method. A gradient-based search algorithm was used to search for the optimal design from the constructed response surface. A comparative analysis showed improvement in energy efficiency by modifying the blade lean instead of blade profile. Falahat [7] made an effort to find the best angle of attack and rotational speed of a flat-blade axial fan. Adeeb et al. [8-10] used formal optimisation techniques to study the effect of different design variables and number of blades on the ceiling fan. However, the investigations fell short of seeing the production line because the jigs and fixtures needed a major overhaul. A common requirement of the production line is to incrementally refine the geometry without any major alteration in the design.

The experimental findings of Rohles et al. [11] reveal that air at  $28^{\circ}\text{C}$  with a running fan will provide the same comfort as air at  $24^{\circ}\text{C}$  without a fan. A major comfort-producing feature is turbulence and variable characteristics of the air plume. Moreover, light objects, loose papers and hairs start to blow at an air speed of 0.8 m/s. Rohles et al. [12] quantified the effect of using a ceiling fan in an open zone at different heights above the floor. It was reported that the air velocity is not affected by the ceiling and is reduced rapidly at almost 40% of the height from the hub.

Son et al. [13] numerically investigated the thermal comfort for a human being standing below the ceiling fan, along with an air conditioner inside the room. The energy consumption during the combined operation of ceiling fan and air conditioner is reduced with the increase in fan speed as compared to the sole operation of air conditioner. Fan air speed is therefore identified as the key factor in thermal comfort and less energy consumption. The effect of energy saving on

thermal comfort at elevated room temperatures was studied by Schiavon and Melikov [14]. Recommendations based on American Society of Heating, Refrigerating and Air-conditioning Engineers standards [15] were taken as the benchmark in carrying out the computational study.

Studies up till now on fan optimisation were either based on experimental or computational approaches. The computational investigations employed mixed techniques by modelling the flow field through Reynolds-Average Navier-Stokes (RANS) algorithm and the fan surface as an actuator surface based on blade-element momentum theory. In this paper the flow field as well as the fan surface was modelled through RANS approach. Moreover, the fan was rotated as a moving reference frame for further design refinement and optimisation studies. Initially, the experimental studies were conducted to analyse the baseline geometry. The standard baseline geometry can be manufactured by various fan manufacturing companies of Pakistan. The performance of the baseline case was gauged against the certified specifications of the government regulatory body. A computational model was developed by the same experimental facility and validated with experimental data. Subsequently, a parametric design study of the fan blades was carried out. Specifically, the effects of rake angle, bend angle and bend position at the root and tip chord were investigated. The optimal design parameters were selected and the blade was fabricated. A comparison between the baseline and optimal blade geometry was carried out based on experimental data. The proposed design satisfies the performance parameters of the government regulatory body. Moreover, the design refinements are carried out without altering the existing production set-up.

## PROBLEM DESCRIPTION AND EXPERIMENTAL STUDIES

### Performance Indicators

There are two common indicators of performance and quality control generally used in Pakistan. Pakistan Standards One (PS-1) is proposed by Pakistan Standards and Quality Control Authority (PSQCA) [16]. The PS-1 should be satisfied for marketing the products locally. For export purpose, separate star-rating criteria are generally adopted. For standard-size ceiling fan, the PS-1 standards are shown in Table 1.

**Table 1.** Performance requirements set by the home appliances regulatory body [16]

PS-1 Standards	
Rated power input (watt)	80 (+10% tolerance)
RAD (m <sup>3</sup> /min.)	220 (-10% tolerance)
Minimum SV (m <sup>3</sup> /min./watt)	3.12 (no tolerance)
Maximum rpm	330 with load

The rated power input (PI) helps the fan motor to rotate at a certain speed. The air velocity profile is recorded at a distance of 1.5 m below the rotary disc of the ceiling fan by taking measurements at several points. The velocity profile is used to assess the spread of velocity from the fan hub to the blade tip. Different velocity profiles can be compared to see the effectiveness of certain design features at various points in the profile. The rated air delivery (RAD) is the volumetric rate of change of air per unit time and is measured in m<sup>3</sup>/min. as per PS-1 standards. It is calculated as:

$$RAD = \pi r^2 \times v_{avg} \times 60 . \quad (1)$$

Here,  $r$  is the radius of fan and  $v_{avg}$  is the average air velocity in m/s. The service value (SV) is the ratio of RAD to power consumption (torque) and is measured in  $\text{m}^3/\text{min.}/\text{watt}$ . For energy efficiency, an increase in SV is desired.

$$SV = \frac{RAD}{Power\ Consumption} \quad (2)$$

The second category of standards is commonly known as star ratings [17], which need to be qualified for export purposes. These ratings are primarily concerned with energy efficiency aspects and are classified with respect to the SV as shown in Table 2.

**Table 2.** Star ratings for export of ceiling fans [17]

Star Rating Index Standards	
Star rating	SV for ceiling fan
1 star	$3.11 < SV < 3.15$
2 stars	$3.16 < SV < 3.32$
3 stars	$3.33 < SV < 3.45$

Torque is the tendency of a force to rotate a body about its axis and is also called the moment of this force. Torque is generated for a specific value of PI. For energy efficiency, torque as well as rated PI should be reduced. Therefore, the energy efficiency in this work is referred to as the RAD to torque ratio. The experiment performed for optimal geometry, obtained from the parametric studies, would meet the power requirements and SV.

### Description of Fan Geometry

Figure 1 shows the conventional configuration of a ceiling fan used as the basis for the studies. A ceiling fan consists of two major parts: hub and blades. The central rotating part to which the blades are attached is called the fan hub. Its purpose is to house an electric motor. The blade section that is attached to the hub is called the blade root, whereas the outermost end is called the blade tip. The diameter of the ceiling fan used in the research for benchmark purposes was 1.42 m, based on the circular area swept by the ceiling fan during operation. The angle between the horizontal plane containing the root chord and the plane midway between the upper and lower surfaces of the blade is known as rake angle, which helps to spread the air. Bend angle is defined as the angle between the two surfaces of the blade. The function of this angle is to push more air downwards in the room, as shown in Figure 1. The leading edge is part of the blade that first contacts the air; alternatively, it is the foremost edge of an airfoil section. The trailing edge of the blade is its rear edge.

The baseline geometry widely used by various manufacturers was selected to get the coordinates of the blade profile. The length of the fan blade was 0.57 m, the chord length at root and tip being 0.16 m and 0.12 m respectively. Aluminum was used to make the blade with a thickness of 0.001 m. The diameter of the fan hub was 0.26 m and the total diameter of the fan including the hub was 1.42 m. The selected fan consisted of three aluminum blades with a bend angle of  $11.8^\circ$  and rake angle of  $5^\circ$ . The bend position at the root and tip chord was 63% and 17% of the chord length

respectively. All the three blades were  $120^\circ$  apart from each other. The experimentally measured fan dimensions are shown in Table 3.

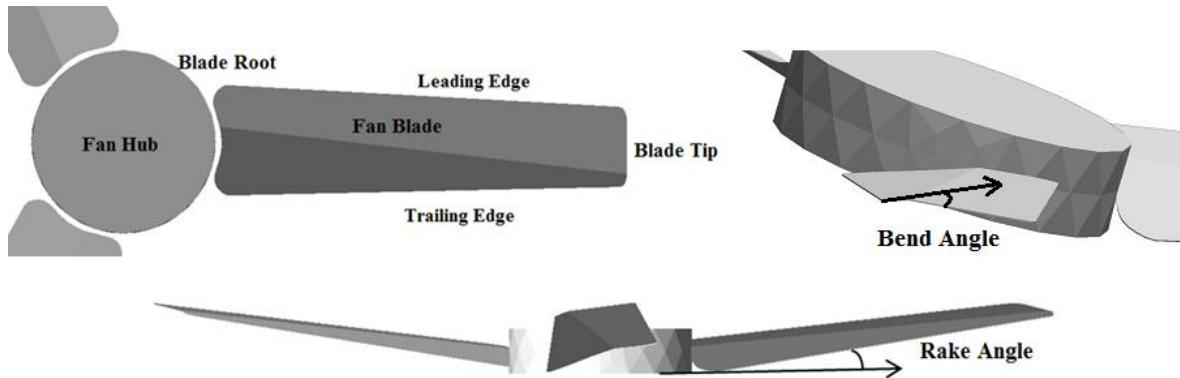


**Figure 1.** Description of fan geometry

**Table 3.** Geometric dimensions of ceiling fan under study

Geometric Attribute	Dimension
Fan hub diameter	0.26 m
Fan blade length	0.57 m
Fan diameter	1.42 m
Fan blade thickness	0.001 m
Fan blade material	Aluminum
Fan blade bend angle	$11.8^\circ$
Fan blade rake angle	$5^\circ$
Fan blade root chord	0.16 m
Fan blade tip chord	0.12 m

### Experimental Set-up and Instrumentation

The experiment to assess the performance of the ceiling fan was carried out in a square room shown in Figure 2. The length, width and height of the test room were 4.5 m, 4.5 m and 3 m respectively. A fan was installed 1 m below the ceiling as shown in Figure 3 – fan distance from the floor was 3 m. A digital inclinometer and bevel protector were used to measure the blade rake, bend and connector angles shown in Figure 4.

The room centre on floor is marked by hanging a thread from fan hub. Two diagonal lines crossing the room centre were drawn on the floor to mark the air velocity measuring points shown in Figure 5. A vane anemometer “PROVA® AVM-07” captured the air velocity magnitude and temperature inside the room. A metal stand, shown in Figure 6, was used to carry the vane anemometer at 1.5 m below the fan. Figure 7 shows the anemometer sensor diameter. The first measuring point was marked as half the diameter of the vane anemometer sensor shown in Figure 8. From the second measuring point, all points were marked equal to the diameter of the sensor. The input/output voltage and current were displayed by an electronic display panel shown in Figure 9. The input voltage was varied through a regulator to set the desired fan speed. A tachometer was hanged above the ceiling fan to capture the rotational speed.

For a fully developed flow, the fan was switched on 2 hours before taking measurements. Seven different rpm settings, 175, 200, 250, 300, 330, 350 and 365, were set for the measurements one by one. For each reading, the anemometer was set on the marked point for 2 minutes so that it could automatically capture the magnitude of maximum velocity. After every measurement, the sensor was placed on the next marked point. It should be noted that the performance of the fan is also dependent on the motor design and associated materials used for fabrication. The core material, winding material and gauge of wires used in inner and outer coils of the motor were all set constant, according to the specifications already used for mass production. Silicon steel sheets were used for the core and a motor with 16 poles was used in this study.

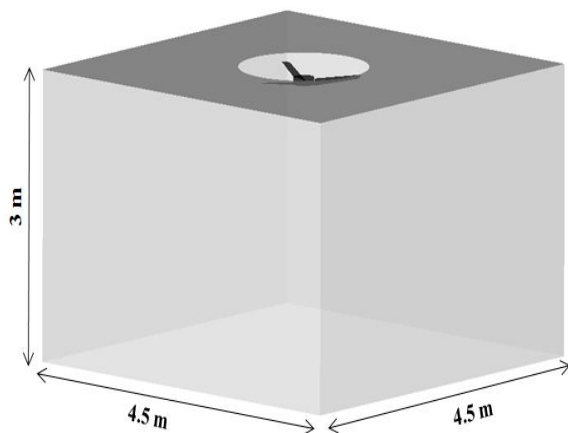


**Figure 2.** Test room

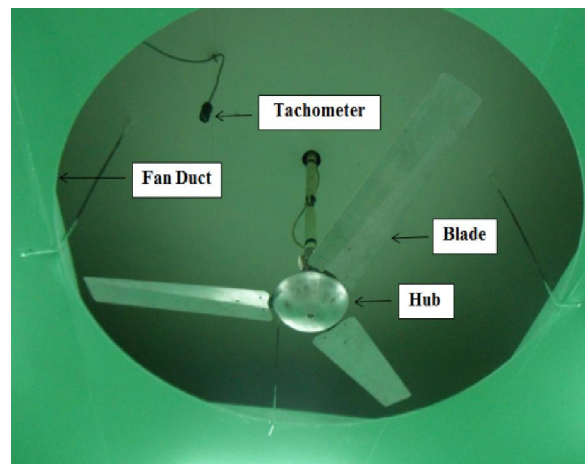


**Figure 3.** Fan duct



**Figure 4.** Bend angle measurement

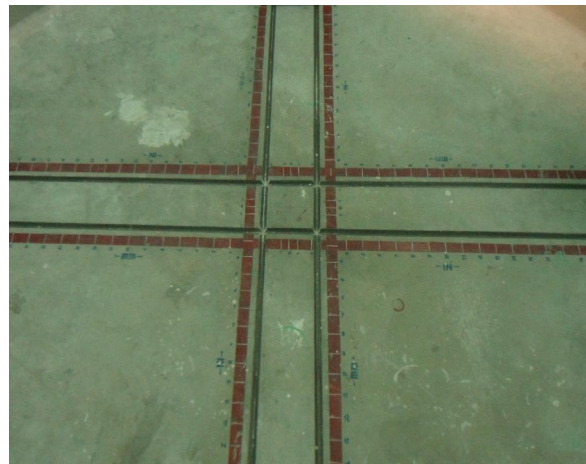


**Figure 5.** Markers for measuring distance



**Figure 6.** Stand for velocity measurement



**Figure 7.** Diameter of anemometer sensor

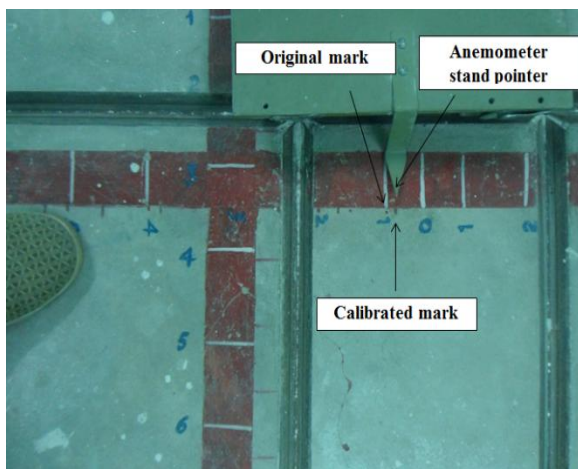


**Figure 8.** Mark points to place anemometer

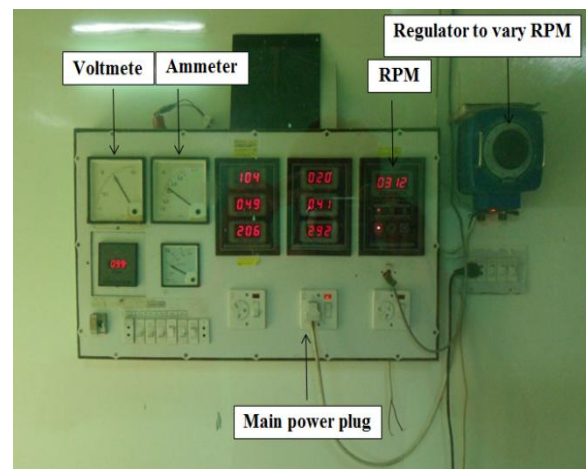


**Figure 9.** Electronic display panel

### Experimental Data Analysis

The experimental data in terms of velocity profiles, voltage, current and power consumption were collected for different fan speeds. The data were subsequently used for comprehending the flow pattern in the room and validating the baseline case. Figure 10 (a) gives a graphical representation of the velocity profile for seven different rpm. The flow patterns clearly show that the velocity is increased from fan hub to blade tip by increasing the fan speed. However, for a certain fan speed, the maximum axial velocity was recorded from 0.2 m to 0.5 m along the blade span. At further than 0.5 m, a sharp decrease in axial velocity was observed. An rpm - power curve (Figure 10 (b)) shows the relationship between fan speed and power; as fan speed is decreased, less power is consumed by the fan motor. Therefore, for energy efficiency, less fan power consumption must be achieved for more RAD.

Table 4 represents an analysis of the baseline fan at different fan speeds compared with desired specifications (PS-1 standards). The motor should consume 80 watts at 330 rpm and should deliver 220 m<sup>3</sup>/min. of RAD. The minimum SV, the ratio of RAD to power consumed by motor, should be 3.12 m<sup>3</sup>/min./watt. For different fan speeds, the power consumption was recorded from 61 watts to 108 watts. It can be observed that at low fan speed, the requirement of RAD was not fulfilled, whereas at high fan speed the power requirement was breached. Moreover, the maximum achievable fan speed should not exceed 330 rpm.

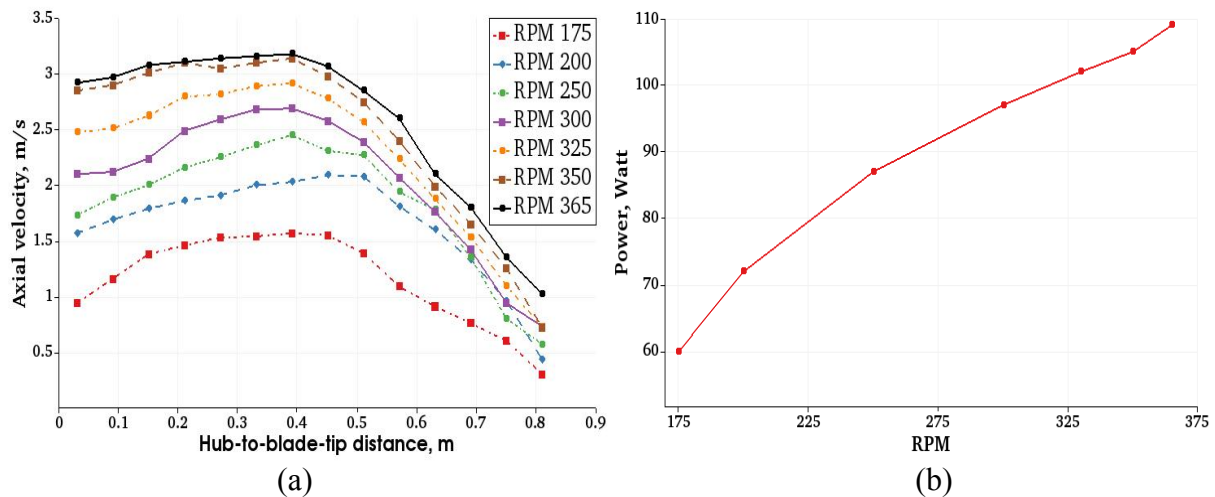


Figure 10. Experimental velocity profiles at different rpm (a) and rpm-power curve (b)

Table 4. Performance indicators at different rpm for baseline geometry

PS-1 Standards		Experimental values						
Maximum speed (rpm)	330	175	200	250	300	330	350	365
Rated power input (watts)	80	61	72	87	97	102	105	108
RAD (m <sup>3</sup> /min.)	220	109	136.9	163.2	194.58	210.2	219.615	231.135
Minimum SV (m <sup>3</sup> /min./watt)	3.12	1.79	1.90	1.88	2.01	2.06	2.09	2.14

## COMPUTATIONAL SET-UP

### Mathematical Modelling

A broad-spectrum utilisation of finite-volume-based algorithms to predict the performance of wind-turbines and turbomachinery blades has been observed during the last two decades. The flow-field induced by the rotation of the ceiling fan blades inside a room is modelled by the incompressible RANS equations. The incompressible Navier-Stokes equation in tensor notation can be expressed as:

$$\frac{\partial u_i}{\partial x_i} = 0 \quad , \quad (3)$$

$$\rho \frac{Du_i}{Dt} = -\frac{\partial P}{\partial x_i} + \frac{\partial \tau_{ij}}{\partial x_j} + f \quad , \quad (4)$$

where  $u_i$  represents the velocity vector,  $\rho$  is the constant fluid density,  $P$  is the pressure,  $\tau_{ij}$  is the stress tensor and  $f$  represents body forces. Eq. (4) indicates that the aerodynamic force is composed of three components, namely pressure, shear stress and body forces.

The RANS equation can be derived from Eq. (4) by resolving the velocity and pressure as time-averaged and fluctuating components:

$$u_i = \bar{u}_i + u'_i \quad p = \bar{p} + p' \quad , \quad (5)$$

where  $\bar{u}_i$  is the mean velocity component and  $u'_i$  represents fluctuation. The chosen averaging method takes the mean value at a fix place in space and averages it over a time span that is large enough for the mean value to be independent of it. The Reynolds stress tensor can be represented as:

$$\tau_{ij,turb} = -\rho \overline{u'_i u'_j} \quad . \quad (6)$$

Substituting Eq. (5) and Eq. (6) in Eq. (3) and Eq. (4) leads to the tensor form:

$$\frac{\partial}{\partial x_i} (u_i) = 0 \quad , \quad (7)$$

$$\rho \left[ \frac{\partial}{\partial t} (u_i) + \frac{\partial}{\partial x_j} (u_i u_j) \right] = -\frac{\partial P}{\partial x_i} + \frac{\partial}{\partial x_j} (\tau_{ij} + \tau_{ij,turb}) \quad . \quad (8)$$

Further, the stress tensor in Eq. (8) is expressed as:

$$\tau_{ij} = \mu \left( \frac{\partial u_i}{\partial x_j} + \frac{\partial u_j}{\partial x_i} - \frac{2}{3} \delta_{ij} \frac{\partial u_k}{\partial x_k} \right) \quad , \quad (9)$$

where  $\delta_{ij}$  is the Kronecker delta. The Reynolds stresses in Eq. (8) are related with the mean velocity gradients using Boussinesq hypothesis:

$$-\rho \overline{u'_i u'_j} = \mu_t \left( \frac{\partial u_i}{\partial x_j} + \frac{\partial u_j}{\partial x_i} \right) - \frac{2}{3} \left( \rho k + \mu_t \frac{\partial u_k}{\partial x_k} \right) \delta_{ij} \quad , \quad (10)$$

where  $\mu_t$  is the turbulent viscosity.

In this study the one-equation Spalart-Allmaras (S-A) turbulence model [18] is used for the modelling of turbulent viscosity for the closure of Eq. (8). The reason for selecting this turbulence model is its minimum deviation of numerical results from experimental data. The S-A model can be expressed as:

$$\frac{\partial(\rho \tilde{\nu})}{\partial t} + \frac{\partial(\rho \tilde{\nu} u_i)}{\partial x_i} = G_\nu + \frac{1}{\sigma_{\tilde{\nu}}} \left[ \frac{\partial}{\partial x_j} \{ (\mu + \rho \tilde{\nu}) \frac{\partial \tilde{\nu}}{\partial x_i} \} + C_{b2} \rho \left( \frac{\partial \tilde{\nu}}{\partial x_i} \right)^2 \right] - Y_\nu + S_{\tilde{\nu}} \quad , \quad (11)$$

where  $G_\nu$  and  $Y_\nu$  represent the production and destruction of turbulent viscosity respectively,  $\sigma_{\tilde{\nu}}$  and  $C_{b2}$  are constants with values 0.667 and 0.622 respectively,  $\nu$  is the molecular kinematic viscosity and  $S_{\tilde{\nu}}$  is a user-defined source term. The last term in Eq. (10) is ignored once the S-A model is used to compute the Reynolds stresses. The term  $\tilde{\nu}$  is identical to the turbulent viscosity except for the near-wall region and is expressed as:

$$\mu_t = \rho \tilde{\nu} \left( \frac{\chi^3}{\chi^3 + C_{v1}^3} \right) \quad , \quad (12)$$

where  $\chi = \tilde{\nu}/\nu$  and  $C_{v1} = 7.1$ .

## Computational Modelling

The ceiling fan geometry includes three blades and a hub in a rotatory disk. The coordinates of geometry were taken from the original model and reproduced in GAMBIT®. For simplicity, the

rivets and connectors were removed in the computational domain because they have negligible effect on the flow. Structured quad map elements were used to mesh the flow field of stationary domain (test room) shown in Figure 11. Unstructured tetrahedral mesh elements were used to mesh the flow field of rotating domain (fan disk). To improve the quality or accuracy of the simulation, a matching grid at the interface of two grid blocks was generated.

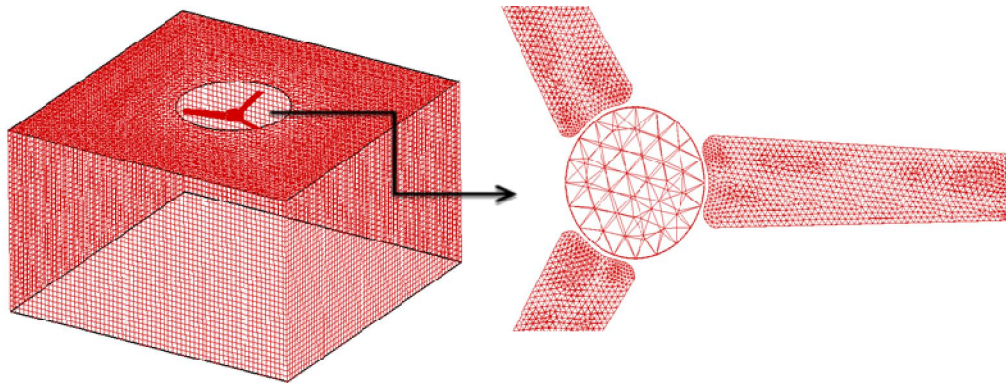


**Figure 11.** Computational domain of fan and room

A grid independence study was carried out by developing grids of three different sizes, as shown in Figure 12. The purpose of grid independence study is to achieve a set of grid points for which the solution and the flow physics of the computational case do not further change if the level of mesh refinement is increased. The grid with the best results in terms of flow profile and computational efficiency was selected for further analysis. For this purpose, three meshes were generated, with cell numbers of 0.5, 0.7 and 2.3 million in coarse, medium and fine grid respectively. All three sets of mesh were computationally solved using the S-A turbulence model. The computational domain has a fine grid near the ceiling fan and a coarse one further away. The grid with 0.7 million cells was selected based on the trade-off between accuracy and computation speed.

After grid selection, a turbulence model sensitivity study was also carried out to compare k-Omega, k-Epsilon and S-A models with experimental data. Results in Figure 13 clearly show that the S-A turbulence model best agrees with experimental values.

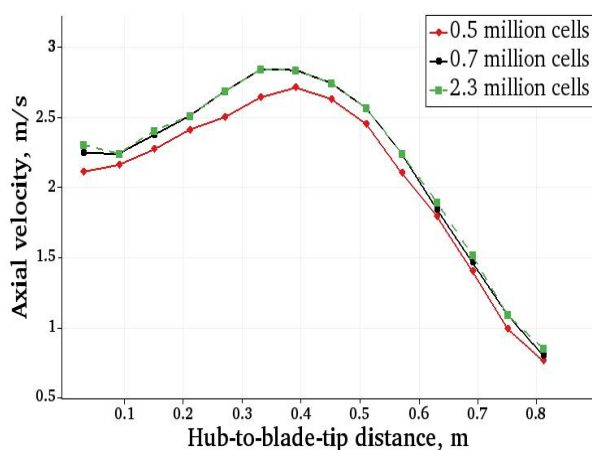


**Figure 12.** Grid independence study

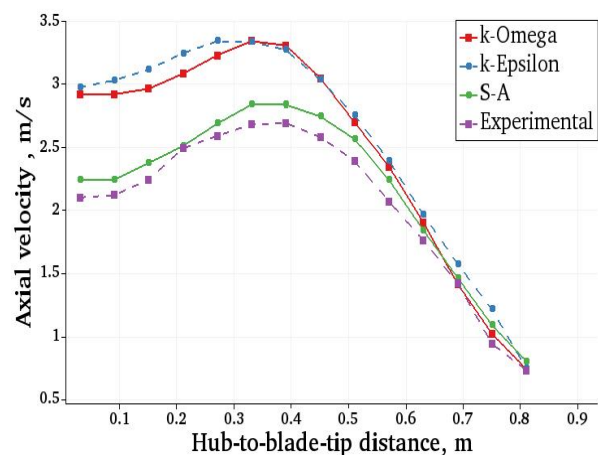


**Figure 13.** Comparison of turbulence models

For the selection of turbulence model, all the computations were performed using the finite-volume code Fluent® with a steady-RANS approach. No-slip velocity or adiabatic wall boundary condition was enforced at the blade surfaces, fan hub and room walls. The pressure, temperature and turbulence intensity was set to 101325 Pa, 288 K and 0.07 % respectively, and the fan speed was set to 300 rpm. The turbulence dissipation rate and momentum discretisation scheme were determined through a first-order upwind scheme. SIMPLE algorithm [19] was used to couple pressure and velocity. A coupled solver was used with an implicit formulation to solve discretised equations and the Courant number was set to 5 for fast convergence.

### Validation Study

A comparison of computational and experimental velocity profiles at 1.5 m below the ceiling fan is shown in Figure 14. Comparison of computational fluid dynamics (CFD) simulations with laboratory tests shows a reasonable fit within 5% bounds of the air velocity behaviour. However, an isolated over-prediction of 6% is observed at approximately 0.4 m of hub-to-blade-tip distance.

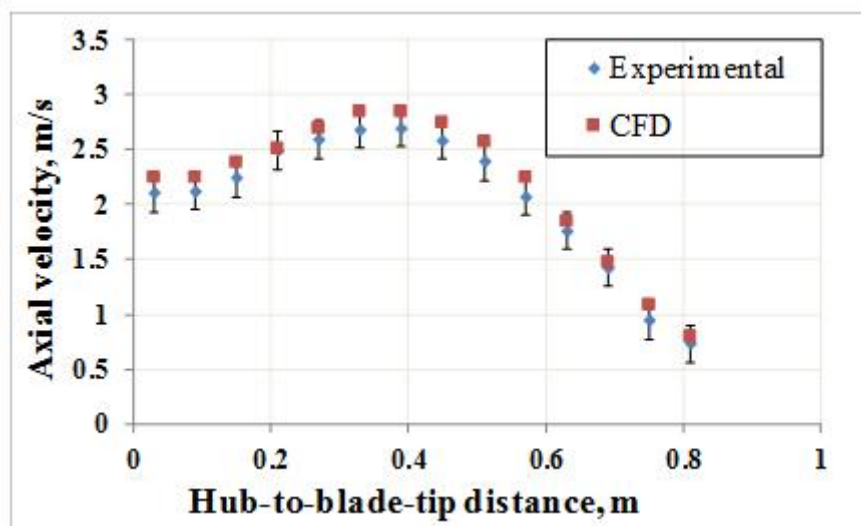
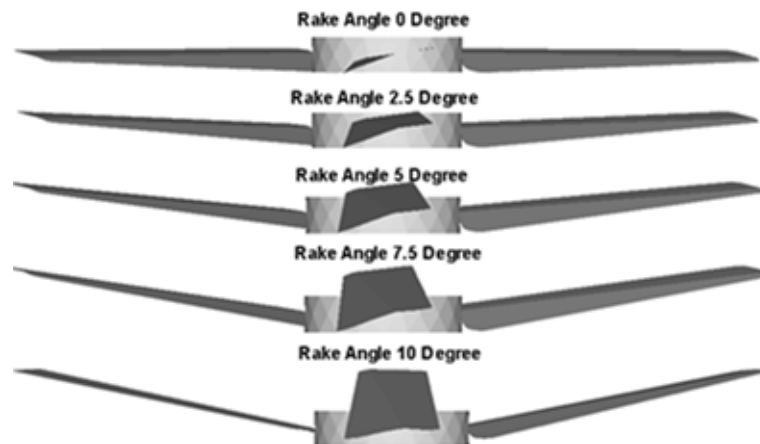


Figure 14. Comparison of experimental and CFD axial velocity at 300 rpm

## RESULTS AND DISCUSSION

### Effects of Rake Angle

The air is found to be pushed downwards typically perpendicular to the plane of rotation of the ceiling fan, the tip vortices being formed near the blade tips. As a result, the air from the lower surface swirls on to the upper surface. It is desired that the fan should have an optimised rake angle so that the flow of air not only is under the fan but also spreads inside the whole domain [20]. However, any compromise on the air delivery is undesirable. All the rake angle studies were conducted at 300 rpm [21] and at nine different angles:  $0^\circ$ ,  $2.5^\circ$ ,  $5^\circ$ ,  $5.5^\circ$ ,  $6^\circ$ ,  $6.5^\circ$ ,  $7^\circ$ ,  $7.5^\circ$  and  $10^\circ$ . The representative geometry is shown in Figure 15.



**Figure 15.** Geometry with different rake angles

The RAD and torque at different rake angles are shown in Figure 16. The higher the fan speed, the higher will be the torque, so to make the fan energy efficient, torque should be reduced with increased air delivery. It can be observed that the RAD keeps on increasing at up to  $6^{\circ}$  angle. If rake angle is more than  $6^{\circ}$ , the air is spread outwards from the diameter of fan rather than on the measuring points. The decrease in RAD above  $6^{\circ}$  can be seen in Figure 16(a). Figure 16(b) presents a reduction trend of torque with increase in rake angle, and at  $10^{\circ}$  there is a sharp reduction in torque. However, it cannot be considered as an optimised value for rake angle because the associated value of RAD is very low.

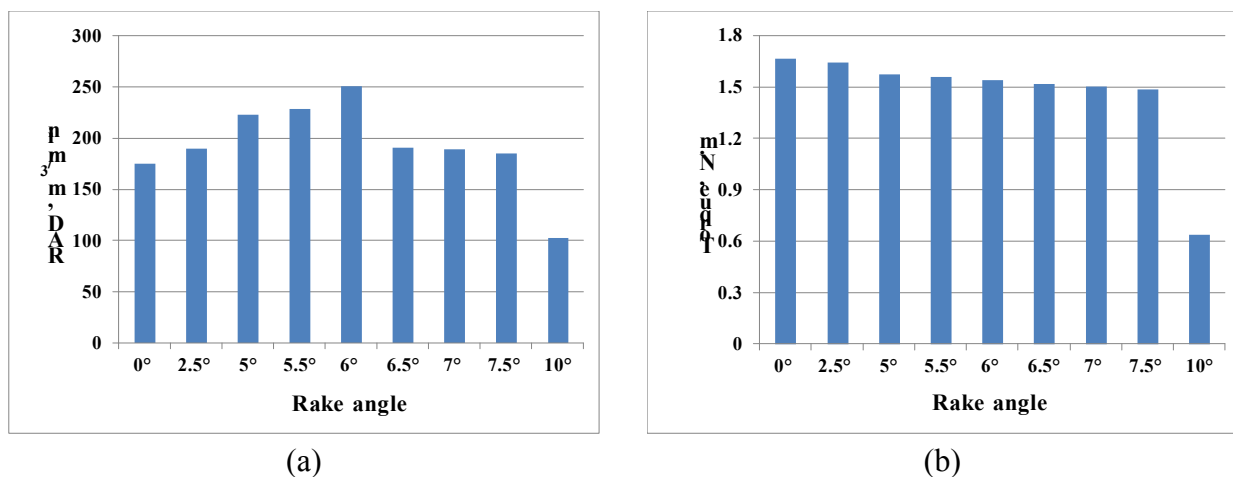


**Figure 16.** Comparison of RAD (a) and torque (b) at different rake angles

### Effect of Bend Angle

The bend angle also plays a key role in ceiling fan performance. The blade bend angle was varied from  $9.8^{\circ}$  to  $12.8^{\circ}$  with an interval of  $1^{\circ}$ , while rake angle was fixed at  $6^{\circ}$  for bend angle study. The simulation was performed at 300 rpm. According to Figure 17, the maximum air velocity is achieved by keeping the bend angle at  $11.8^{\circ}$ .

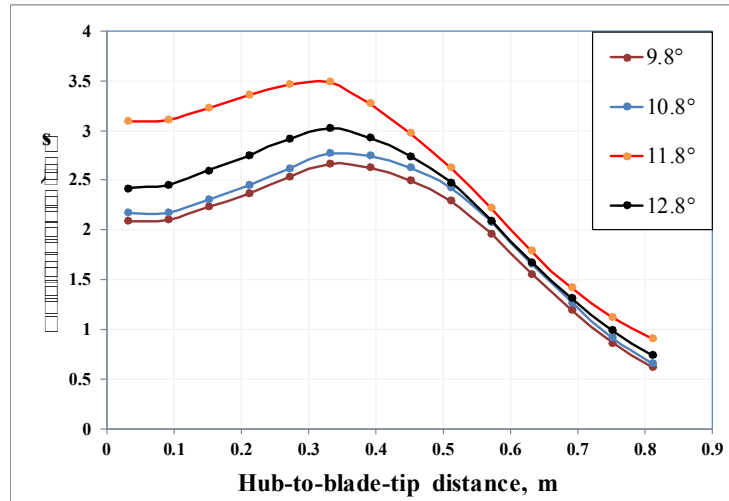


Figure 17. Comparison of axial velocity at different bend angles

**Bend Position Studies**

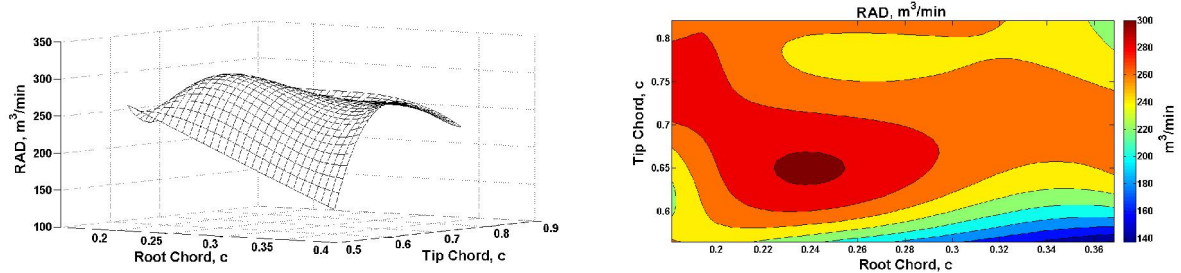
The bend position significantly governs the ceiling fan performance. In this work the bend position at the root and tip was varied around the baseline values. Specifically, oblique variation in the bend position along chord was performed. For each blade shape the air velocity, mass flow rate, RAD, torque and energy efficiency are briefly explained. For oblique bend position variation, different root and tip chord positions were uniformly varied. A 4×4 matrix was created and a total of sixteen types of geometry, divided into 4 groups, were simulated as shown in Table 5. The range of the matrix was determined keeping in view the production line flexibility.

Table 5. Bend position variations

Root ↓ Tip Chord →	0.56c	0.64c	0.72c	0.82c
0.18c	Geometry 1	Geometry 2	Geometry 3	Geometry 4
0.24c	Geometry 5	Geometry 6	Geometry 7	Geometry 8
0.30c	Geometry 9	Geometry 10	Geometry 11	Geometry 12
0.36c	Geometry 13	Geometry 14	Geometry 15	Geometry 16

Note: c = chord length of blade

After extracting the results, a cubic spline interpolation was used in MATLAB® to find the optimised geometry, which was selected based on the simulated cases. The result shows that the optimised fan blade has improved the RAD with reduced torque values as compared to the baseline. Figure 18 shows a surface plot of the RAD and associated contour plot, clearly identifying the region of maxima. The RAD, also known as volume flow rate, was plotted as a function of root and tip chord. The contour plot shows that maximum RAD is in the region containing the root chord between 0.23c - 0.25c and the tip chord between 0.63c - 0.67c. The contour colours differentiate the intensity of the RAD at different tip and root chord positions.



**Figure 18.** RAD surface plot (left) and contour plot (right) for various bend positions

The behaviour of associated mechanical torque is shown in Figure 19. The inclination increases as the bend position is moved towards the leading edge of root and tip chord. The mechanical torque is also mapped on a two-dimensional contour plot in Figure 19. The results indicate that the magnitude of the torque linearly increases as the bend position at the root and tip chord increases. Contour colours are shown to differentiate the intensity of torque.

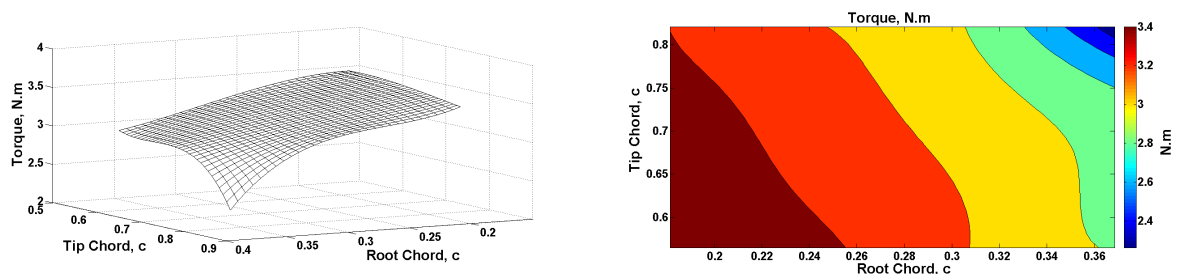


**Figure 19.** Torque surface plot (left) and contour plot (right) for various bend positions

The surface plot of energy efficiency (air delivery to torque ratio) is plotted in Figure 20 as a function of root and tip chord. The maximum value is at root chord of 0.24c and tip chord of 0.64c. One peak is at root chord of 0.37c and tip chord of 0.9c, which cannot be considered because of poor RAD as shown in Figure 20. The associated contour plot indicates that the magnitude of energy efficiency is maximum at root chord of 0.24c and tip chord of 0.64c.

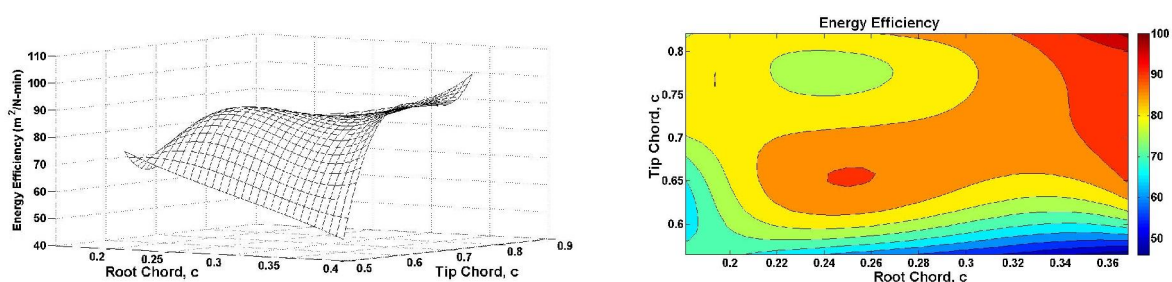


**Figure 20.** Energy efficiency surface plot (left) and contour plot (right) for various bend positions

### Comparison of Baseline Geometry and Proposed Modification

The comparison between the baseline geometry (Table 3) and the modified one is shown in Figure 21. The final design is selected based on the parametric analysis of this particular industrial problem in order to improve the performance of ceiling fans. The modified ceiling fan-blade geometry contains a root chord of 0.24c and tip chord of 0.64c ('Geometry 6' in Table 5).



**Figure 21.** Comparison of baseline geometry and proposed modification of blade design

A numerical comparison between the flow fields is shown in Figure 22. Velocity contours in mid-plane of the room at 300 rpm present the distribution of air velocity. The velocity field is represented by streamlines on the filled background with colours proportional to the air speed. The airflow passes through the ceiling fan disk and goes straight down vertically. As the airflow approaches the middle part of the room, the momentum loss causes the flow to circulate and spread outwards. However, since the blades are of finite span, minor flow circulation near the tip of the ceiling fan is also observed. The magnitude of the air circulation below the fan disk is significantly higher for the modified geometry. It should be noted that besides the increase in vertical velocity below the ceiling fan, a significant spread of airflow along the breadth of the room is also observed. Therefore, the modified geometry exhibits improved airflow characteristics in terms of downward intensity and breadth as well.

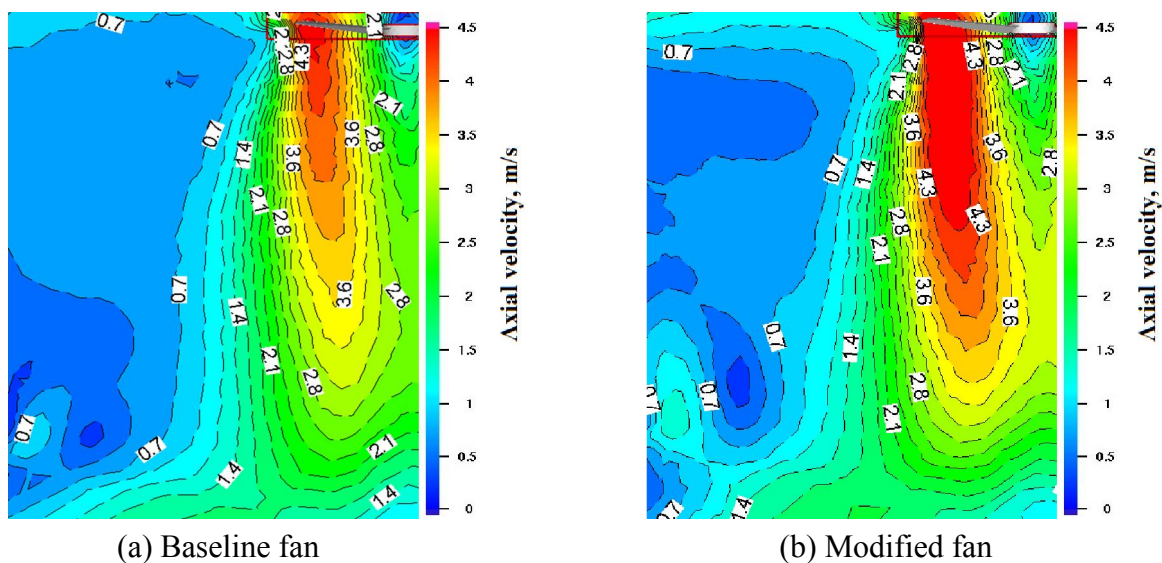


**Figure 22.** Comparison of velocity contours

The static pressure contour plots of the upper surface of the baseline geometry and the proposed modification are compared in Figure 23. The static pressure values are represented with colours proportional to their magnitude. The reduction in static pressure is observed from hub to tip along the span of the blade. The low-pressure region near the tip is associated with the flow swirl from the lower surface to the upper surface of the fan blade. The swirl generates tip vortices, a typical feature of the finite wing theory. Moreover, a sudden decrease in pressure along the bend line is evident for both types of geometry. It can be seen that the low-pressure regions over the

upper surface of the blade are more pronounced in the modified case. This is attributed to the forward shift of the root and bend positions along the chord.

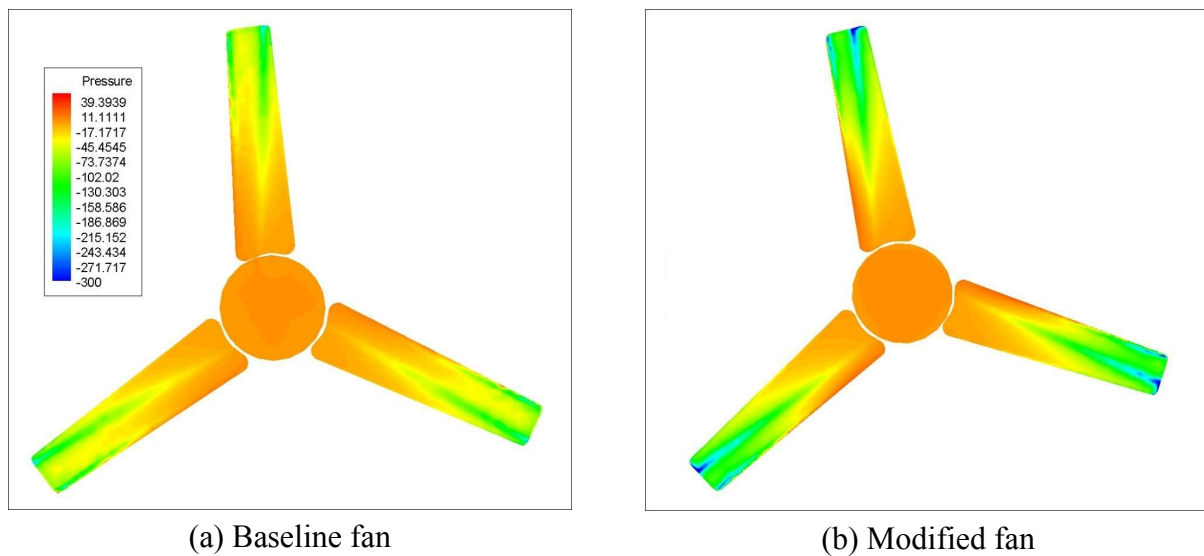


**Figure 23.** Upper surface static pressure contour of fan blades (counter-clockwise rotation)

The final optimum design was tested for experimental verification purposes. The final blade sets with optimum setting of geometric parameters were manufactured using available manufacturing set-up. Using the same ceiling fan testing lab, which was used for reference blade, the fan was tested with the final blade design. Table 6 shows a comparison of performance between the baseline and modified cases from experimental data. The data are collected at different fan speeds and the considered key performance indicators are RAD, power consumed and SV. The baseline geometry meets the specifications of RAD and power at 365 rpm. The specific values of RAD and power are 231 m<sup>3</sup>/min. and 108 watts respectively. The proposed modification has an RAD and power of 235 m<sup>3</sup>/min. and 76 watts respectively at 300 rpm.

**Table 6.** Performance analysis under different rpm

Performance Indicator	RPM											
	250			300			330			365		
	Base.	Mod.	% Imp.	Base.	Mod.	% Imp.	Base.	Mod.	% Imp.	Base.	Mod.	% Imp.
RAD	163.2	180.7	10.72	194.58	235.1	20.82	210.2	259.3	23.36	231.1	302.5	30.88
Power	87	66	24.14	97	76	21.65	102	81	20.59	108	89	17.59
SV	1.88	2.74	45.95	2.01	3.09	54.21	2.06	3.20	55.34	2.14	3.40	58.82

Note: Base. = Baseline; Mod. = Modified; Imp. = Improvement

Improvements in terms of the percentage of different performance indicators are shown in Figure 24. The improvement in RAD and SV increases with fan speed. However, the power consumption is reduced as fan speed increases. This decrease in power consumption is attributed to

the associated decrease in torque. It should be noted that the maximum achievable fan speed by the ceiling fan motor hovers around 365-370 rpm for different blades.

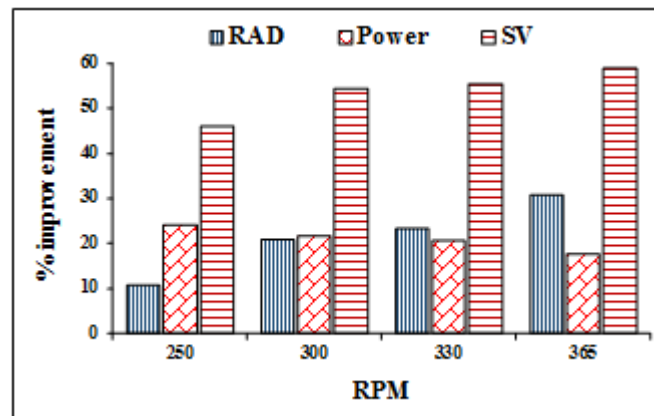


**Figure 24.** Improvements in performance indicators with RPM

## CONCLUSIONS

In this research work a systematic evaluation has been carried out to make the ceiling fan more energy efficient. A modified fan blade geometry is obtained through a parametric study of the blade, which is fabricated on the existing production line without any alteration. The experimental verification of the modified geometry indicates that a 300 rpm scenario qualifies for all the desired specifications. An increase in RAD and SV and decrease in power consumption are achieved. Specifically, improvements of 21% in RAD, 22% in power consumption and 54% in SV are attained with the proposed modification.

## ACKNOWLEDGEMENTS

The authors would like to thank Malik Izhar Awan of StarCo Fans®, Gujrat, Pakistan for fruitful discussions and sharing resources related to this work. Valuable input from Dr. Khalid Parvez and Dr. Abdul Ghafoor is appreciated. The work was supported by the Higher Education Commission (HEC), Pakistan (Grant No. PD-IPFP/HRD/HEC/2013/1943).

## REFERENCES

1. A. Jain, R. R. Upadhyay, S. Chandra, M. Saini and S. Kale, "Experimental investigation of the flow field of a ceiling fan", Proceedings of ASME Heat Transfer/Fluids Engineering Summer Conference, **2004**, Charlotte, USA, pp.93-99.
2. K. Schmidh and D. J. Patterson, "Performance results for a high efficiency tropical ceiling fan and comparisons with conventional fans: Demand side management via small appliance efficiency", *Renew. Ener.*, **2001**, 22, 169-176.
3. R. Bassiouny and N. S. Korah, "Studying the features of air flow induced by a room ceiling-fan", *Ener. Buil.*, **2011**, 43, 1913-1918.
4. Y. Momoi, K. Sagara, T. Yamanaka and H. Kotani, "Modeling of ceiling fan based on velocity measurement for CFD simulation of airflow in large room", Proceedings of 9<sup>th</sup> International Conference on Air Distribution in Rooms, **2004**, Coimbra, Portugal, pp.145-150.

5. D. S. Parker, H. S. Guan and D. H. Bart, "High efficiency ceiling fan", *US Patent 60 39,541* (2000).
6. K. S. Lee, K.-Y. Kim and A. Samad, "Design optimization of low-speed axial flow fan blade with three-dimensional RANS analysis", *J. Mech. Sci. Technol.*, **2008**, *22*, 1864-1869.
7. A. Falahat, "Numerical and experimental optimization of flow coefficient in tubeaxial fan", *Int. J. Multidiscipl. Sci. Eng.*, **2011**, *2*, 24-29.
8. E. Adeeb, A. Maqsood, A. Mushtaq and Z. Hussain, "Shape optimization of non-linear swept ceiling fan blades through RANS simulations and Response Surface Methods", Proceedings of 12<sup>th</sup> International Bhurban Conference on Applied Sciences and Technology, **2015**, Islamabad, Pakistan, pp.385-390.
9. E. Adeeb, A. Maqsood, A. Mushtaq and C. H. Sohn, "Parametric study and optimization of ceiling fan blades for improved aerodynamic performance", *J. Appl. Fluid Mech.*, **2016**, *9*, 2905-2916.
10. E. Adeeb, A. Maqsood and A. Mushtaq, "Effect of number of blades on performance of ceiling fans", Proceedings of 4<sup>th</sup> International Conference on Advances in Mechanics Engineering, **2015**, Madrid, Spain, Art. no. 02002 .
11. F. H. Rohles, S. A. Konz and B. W. Jones, "Ceiling fans as extenders of the summer comfort envelope", *ASHRAE Trans.*, **1983**, *89*, 245-263.
12. F. H. Rohles Jr., J. E. Laviana and T. E. Shrimplin, "Assessing air velocities from the industrial ceiling fans", *ASHRAE Trans.*, **1986**, *92*, 288-305.
13. S. H. Ho, L. Rosario and M. M. Rahman, "Thermal comfort enhancement by using a ceiling fan", *Appl. Thermal Eng.*, **2009**, *29*, 1648-1656.
14. S. Schiavon and A. K. Melikov, "Energy saving and improved comfort by increased air movement", *Ener. Buil.*, **2008**, *40*, 1954-1960.
15. ASHRAE, "ASHRAE Standard 55: Thermal Environment Conditions for Human Occupancy", American Society of Heating, Refrigerating and Air-Conditioning Engineers Inc., Atlanta, **2005**.
16. T. Tauqeer, M. A. Ansari and A. Hasan, "Realization for low cost and energy efficient ceiling fans in the developing countries", *Renew. Sust. Ener. Rev.*, **2017**, *76*, 193-201.
17. National Energy Efficiency and conservation Authority, "Energy Standards & Labeling scheme", **2016**, <http://www.enercon.gov.pk> (Accessed: November 2016).
18. P. R. Spalart and S. R. Allmaras, "A one-equation turbulence model for aerodynamic flows", Proceedings of *AIAA 30<sup>th</sup> Aerospace Sciences Meeting and Exhibit*, **1992**, Reno (NV), USA.
19. H. K. Versteeg and W. Malalasekera, "An introduction to computational fluid dynamics", 2nd Edn., Pearson Education Limited, Harlow, **2007**, pp.186-211.
20. R. Aynsley, "Circulating fans for summer and winter comfort and indoor energy efficiency", Environment Design Guide (Australian Institute of Architects), Melbourne, **2007**.
21. M. A. Afaq, A. Maqsood, K. Parvez and A. Mushtaq, "Study on the design improvement of an indoor ceiling fan", Proceedings of 11<sup>th</sup> International Bhurban Conference on Applied Sciences and Technology, **2014**, Islamabad, Pakistan, pp.279-283.